P. Molesini, G. Gori, A. Guardone
An Analysis of Fast-Response Pressure Probes Dynamics for ORC Power Systems
Energy Procedia, Vol. 129, 2017, p. 264-271
doi:10.1016/j.egypro.2017.09.152

Available online at www.sciencedirect.com

ScienceDirect

Energy Procedia 129 (2017) 264–271

Energy Procedia

www.elsevier.com/locate/procedia

IV International Seminar on ORC Power Systems, ORC2017
13-15 September 2017, Milano, Italy

An analysis of fast-response pressure probes dynamics for ORC power systems

P.Molesini, G.Gori, A.Guardone*

Department of Aerospace Science & Technology, Politecnico di Milano, Via La Masa 35, 20156 Milano, Italy

Abstract

The dynamic response of line-cavity systems in ideal and non-ideal compressible-fluid conditions is investigated numerically using the SU2 open-source suite for multi-physics simulations. The response of the system is studied for small but finite pressure perturbations, to predict the behaviour of fast-response pressure probes in turbomachinery for gas and ORC power systems. The probe step-response is found to present significant damping due to non-linear wave propagation. Non-idealities in the close proximity of the liquid-vapour curve increase the signal damping due to non-monotone variations of the speed of sound. A simplified approach is proposed to predict the probe dynamic characteristics in ideal regime. The estimation of the probe dynamics in non-ideal regime is found to be very critical and to strongly depend on the thermodynamic state of the fluid. The present results provides a guideline for the design of fast-response pressure probes to be used e.g. past the rotor stage of ORC turbine vanes.

Peer-review under responsibility of the scientific committee of the IV International Seminar on ORC Power Systems.

Keywords: Non-ideal Compressible-Fluid Dynamics, Fast-response pressure probes, Line-cavity systems, SU2, ORC power systems

1. Introduction

Time resolved measurements of fluid properties in Organic Rankine Cycle (ORC) power systems operating in highly non-ideal conditions are fundamental to investigate the complex flowfield that develops through a turbomachinery cascade. Unsteady phenomena, such as, for instance, vortex shedding or pressure fluctuations related to the wake of rotating blades, play a key role in determining the efficiency of the stage and they possibly result in undesired noise and thermal stresses [1]. Due to the high rotational speed of blade cascades that characterize most of the conventional turbomachinery applications, fast-response pressure probes are required to capture flow velocity and pressure fluctuations within a wide bandwidth which spans from very low frequencies to up to several kHz, which corresponds to the frequency of typical flow unsteadiness past a rotor cascade [2–6].

The development of fast-response pressure probes profited of micro piezo-resistive sensors and flow reconstruction techniques, which allowed to resolve the flow field by means of multiple measurements taken at different times and

* Corresponding author.
E-mail address: alberto.guardone@polimi.it

1876-6102 © 2017 The Authors. Published by Elsevier Ltd.
Peer-review under responsibility of the scientific committee of the IV International Seminar on ORC Power Systems.
10.1016/j.egypro.2017.09.152

positions [7]. To enhance the strength of the probe frame, a possible choice is to encapsulate the piezo-resistive sensor within the probe head. This solution guarantees a more robust probe but, as a consequence, it implies that the time response of the instrument suffers from a delay due to the dynamics of the line-cavity system which connects the external domain to the piezo-resistive transducer. Since the dynamic of the piezo-resistive transducer is usually much faster than that of the line-cavity system, geometrical design of the probe and the properties of the fluid have a major influence on the overall time response [8]. Analytical models which are currently available to predict the dynamic response of line-cavity systems to a given perturbation rely, in general, on the acoustic wave assumption, i.e. they model the system response to weak perturbations. Moreover, analytical models are built on the ideal gas assumption, meaning that the gas obeys the Ideal Gas law $Pv = RT$, whereas ORC power systems employ a special class of fluids that, for a certain set of thermodynamic states, may exhibit non-ideal features. Ideal and non-ideal thermodynamic regimes can be identified through the value of the fundamental derivative of gas-dynamics $\Gamma = 1 + (\partial c/\partial P)_s/(\rho c)$ [9]. This quantity depends on both the molecular complexity and the thermodynamic state of the fluid, and it is greater than one in the so-called ideal dilute gas regime. Otherwise, when the value of Γ is positive and below unity, the state of the fluid lies in the non-ideal regime, which is characterized by many unconventional thermodynamic phenomena, such as for example a negative variation of the speed of sound of the fluid following a positive pressure perturbation. Besides the intensity of the perturbation, a non-monotone dependency of the speed of sound from the value of temperature may further affect the dynamics characteristics of the probe [10].

This paper is focused on the investigation of analytical non-linear models when strong perturbations, like for instance shock waves, are involved. Moreover, the aim of this work is to provide a correlation to estimate the effects of non-linear wave propagation in terms of signal damping. To provide a qualitative guideline to design fast-response pressure probes to be used in ORC power systems, the investigation is extended to the non-ideal regime. The time response of an exemplary line-cavity system is reconstructed numerically using the non-ideal solver included in the open-source software suite SU2 [11,12]. The system is first introduced and tested with dilute air to determine its characteristics in terms of geometrical factors and dynamics characteristics. Later, the same geometry is studied using MDM (Octamethyltrisiloxane $C_8H_{24}O_2Si_3$) as working fluid. The improved Peng-Robinson Stryjek-Vera (iPRSV) Equation of State (EoS) is employed to provide a description of the fluid thermodynamic behavior within the non-ideal regime. To highlight differences, numerical simulations are carried out for two different operating conditions representative of an ideal and a non-ideal flow regime.

This work is organized as follows: section 2 presents analytical models for line-cavity systems. In Section 3, numerical results, regarding predictions for both dilute-air and MDM, are presented. Finally, section 4 presents a brief conclusion.

2. Analytical models for line-cavity systems

The knowledge of the dynamic characteristics of each instrument is key to properly choose the tool that suits the particular measurement process at best. The measure of pressure within an unsteady flow domain characterized by harmonic fluctuations at high frequencies, such as the one past a rotor in turbomachinery applications, requires a fast-response probe. The bandwidth of the instrument defines the range of frequencies for which the system returns a reliable output. To establish the maximum frequency that can be correctly captured by a given measurement system, dynamic calibration must be carried out. This crucial step is mandatory since analytical models are commonly based on a simplified description of the actual geometry of the probe. Moreover, numerical simulations do not account for flaws due to the manufacturing process. Nevertheless, numerical simulations and/or analytical models are particularly beneficial to the design process. For instance, analytical models may be tuned on experimental data and used for estimating the probe dynamic behavior in operating conditions other than those of the experiment. Furthermore, such tools may help to estimate the dynamic characteristics of diverse geometrical configurations for a wide range of thermodynamic conditions, in particular when experiments are difficult and expensive, e.g. in highly non-ideal conditions such as those experienced in ORC power systems.

2.1. Analytical modeling

The analytical models currently available are based on mechanical or electrical analogies [13]. They usually describe the line-cavity system as a second-order linear system, providing the value of the resonant frequency and the non-dimensional damping factor. The system is described as a damped harmonic oscillator where the mass corresponds to the amount of fluid contained within the line and the mechanical compliance is related to the compressibility of the fluid within the cavity. Damping is usually modeled via a resistance factor, retrieved by the analytical solution of the two-dimensional viscous equation for laminar flows [13]. For instance, the Hougen model [13] gives:

$$f_{res} = \frac{c}{2\pi(L+\delta)\sqrt{\frac{V}{SL}+\frac{1}{2}}}, \qquad \xi_v = \frac{2\nu}{S\,f_{res}}, \tag{1}$$

where ρ, c and ν are respectively the density, the speed of sound and the kinematic viscosity of the fluid in the current measurement conditions. L is the length of the line, S is the line cross section, V is the volume of the cavity and δ is the so-called *end-line* correction [14], a parameter used to take into account the inertia of the fluid within the line. As for the vast majority of analytical models, Eq. (1) holds under the acoustic assumption, i.e. non-linear terms are not taken into account. However, pressure signals measured by fast-response pressure probes may suffer from significant unforeseen damping if pressure perturbations are not infinitesimal (see e.g. [8]). This could warp the predicted dynamic response and could ultimately translate into an incorrect design.

2.2. Non-linear damping in line-cavity systems

If the external thermodynamic state undergoes a step perturbation of intensity ΔP to the initial value of pressure P, acoustic waves (or shocks, for larger intensities) propagate through the line into the cavity. Most line-cavity models are derived from the 1D momentum equation integrated over the line, which gives [15]:

$$\frac{d^2P}{dt^2} + \left[\frac{1}{2}\frac{c\Delta M}{(L+2\delta)} + \frac{8\pi\nu}{S}\right]\frac{dP}{dt} + \frac{S\,c^2}{(L+2\delta)V}P = \beta P, \tag{2}$$

where $\beta = (P+\Delta P)/P$ and ΔM is the Mach number variation across the wave. Viscous contribution to damping reduces to the expression presented in Eq. (1). The latter generally provides unrealistically small values if applied to estimate viscous non-dimensional damping factor of fast-response pressure probes operating in typical turbomachinery plants. For instance, the Hougen model would prescribe a non-dimensional damping factor of 0.008 for a probe characterized by a resonant frequency of 50 kHz and a line diameter of 0.3 mm (e.g. the sensor presented in [8]) operating with dilute air in standard conditions. On the other hand, the Mach number variation ΔM may increase significantly as β increases, determining a larger value of damping due to non-linear terms.

Although inaccurate for shock waves propagation, the line impedance relation $\Delta M = \Delta P/(\rho c^2)$ represents a simple way to define a conservative relation between the Mach number variation and the pressure perturbation entering the line-cavity system, as it provides larger values than those obtained from the Rankine-Hugoniot relations. Therefore, the non-dimensional damping factor due to non-linear convective terms is expected to increase as $\Delta P/(\rho c^2)$ increases. However, the overshoot of the pressure signal decreases as ξ increases. By considering the rough approximation $\xi_{nl} = \eta\Delta P(1-\xi)/(\rho c^2)$ yields,

$$\xi_{nl} = \frac{\eta\frac{P}{\rho c^2}(\beta-1)}{1+\eta\frac{P}{\rho c^2}(\beta-1)}, \tag{3}$$

where η is a factor that depends on the geometry and setting of the probe and the viscous damping is neglected ($\xi \simeq \xi_{nl}$). It shall be noted that the ratio $P/(\rho c^2)$ (associated to the isentropic compressibility of the fluid) reduces to $1/\gamma$ under the polytropic, constant-specific-heat ideal gas model, where γ is the specific heat ratio.

3. Results

The considered line-cavity design is reported in figure 1a and is employed in all simulations presented throughout this paper. The shape of the cavity is properly chosen to be as simple as possible and aims at avoiding flow separation

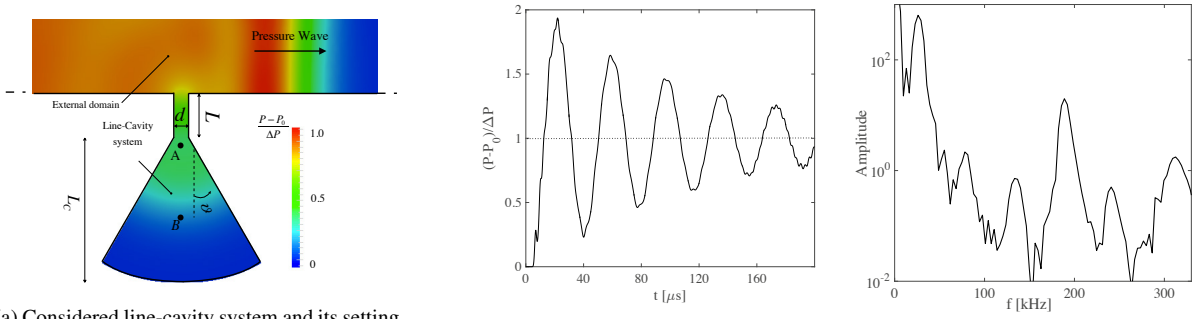

(a) Considered line-cavity system and its setting. CFD results are plotted at $t = 6\ \mu s$: the wave enters the cavity and weakens.

(b) Non-dimensional step-response with dilute air: step value is 1.001 the operating pressure.

(c) Step-response amplitude spectrum.

Fig. 1: geometrical sketch of the considered line-cavity system design (a). Floats (b) and (c) reports the step-response for dilute air and the corresponding amplitude spectrum.

and vortex shedding. The length of the cavity L_C is 1.0 mm, the cavity length to line length ratio is 3.33, the line diameter to line length ratio is 0.1 and the θ angle is 30°. The line axis is normal to the mean direction of the external flow field, i.e. the static pressure is measured. A large portion of the external domain is included in the computational domain to take into account the influence of the external flow-field in the close proximity of the line inlet. The pressure signal, as measured at the center of the cavity (node B), will be considered as the quantity of reference in the analysis. The intensity of the incoming pressure wave is represented by the pressure ratio β.

SU2 capabilities in reproducing the unsteady flow field within a line-cavity system excited by a pressure perturbation was already assessed in [10] where the predicted response is compared against experimental data. As in [10], a two-dimensional approximation of the domain is used. Numerical simulations are carried out under the inviscid fluid assumption. For all the simulations presented hereinafter, the domain is discretized through unstructured grids. A backward Euler scheme with a dual-time-stepping method is used for the unsteady term while Roe scheme is employed for the computation of the convective fluxes for the pseudo-time problem.

3.1. Ideal flow

The step-response to a small acoustic pressure perturbation ($\beta = 1.001$) is reconstructed for air in standard conditions ($P = 1$ bar, $T = 290$ K). A time-step of 0.15 μs is chosen to evolve the solution in time over a numerical grid containing 50 000 triangular elements (the convergence of the solution was verified using both coarser and finer grids). Figure 1b reports the output pressure signal, as measured in time at point B, and scaled by the applied step value. The shape of the predicted time response resembles the one typical of an under-damped second-order system. A second-order identification based on ARX algorithm [16] provides a resonant frequency of 25.7 kHz and a non-dimensional damping factor of 0.055, whereas the analytical expression (1) prescribes a resonant frequency of 30.6 kH and a non-dimensional damping factor due to viscous terms of 0.019. Differences between the numerical results and the analytical model are possibly due to the particular chosen design and setting, as described in [10]. The amplitude spectrum of the step-response is presented in Figure 1c. A Hanning window is applied and the observation time is 200 μs. The main frequency peak is placed at 25.7 kHz, but the spectrum of the signal is characterized by a high-frequency peak at about 192 kHz, which is believed to be associated to the acoustic wave reverberation within the cavity. These harmonic fluctuations cannot be modeled under second-order approximations. However, the amplitude of these secondary harmonics is one order of magnitude smaller than that of the fundamental and their frequency is far from the resonant frequency. Therefore, for this particular case, the contribution of secondary harmonics on the overall pressure signal is negligible.

The time response of the probe is studied beyond the limit of acoustic waves, i.e. for large values of β. Several numerical simulations were performed to reproduce the behavior of the considered system, for different values of β,

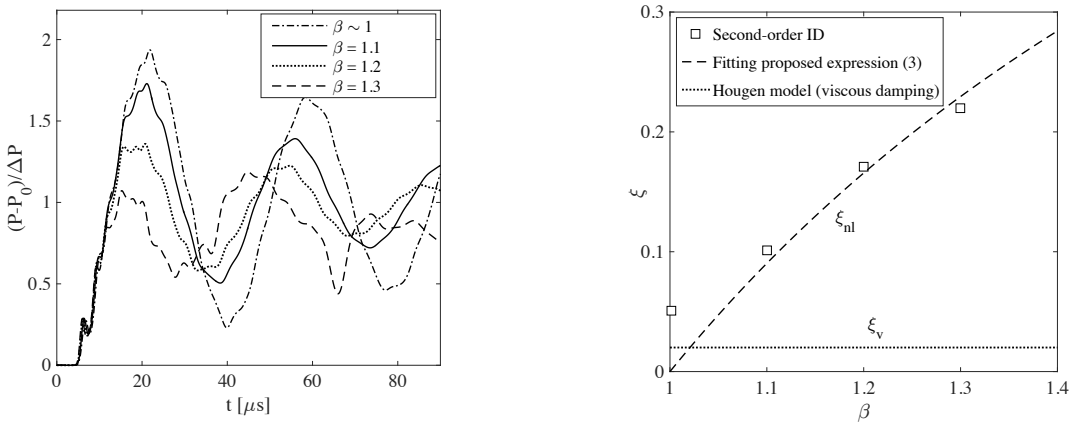

(a) numerical step-responses for different values of pressure ratio β.

(b) Non-linear damping factor trends vs pressure ratio β.

Fig. 2: Step-responses as computed numerically for different values β (a). Values of the non-dimensional damping factors, resulting from a second-order system identification on the output pressure signal, are plotted against β (b).

considering air at fixed operating conditions. Numerical results provide evidences that the non-linear damping, and therefore the intensity of the initial perturbation, impacts significantly on the dynamics of the line-cavity system. For instance, figure 2a presents the non-dimensional step-response of the probe for an increasing value of the perturbation strength ($\beta \sim 1.0, \beta = 1.1, \beta = 1.2, \beta = 1.3$). The pressure is scaled by the intensity of the perturbation. Numerical results shows that the non-dimensional characteristic frequency slightly increases as β increases while the damping of the signal increases with β. This entails larger rising times as β increases, i.e. slower probe responses. Second-order identification provides reference values of the non-dimensional damping factor for different β. Numerical results clearly suggest that the damping grows critically as the intensity of the perturbation increases. Numerical results are compared in Figure 2b against the viscous damping factor predicted by the Hougen model and by the proposed expression (3). The Hougen model fails as the acoustic wave assumption is relaxed whereas curve (3) fitted using $\eta = 1.388$ (dashed line in Figure 2b) is capable of reproducing the qualitative behavior. The time response was reconstructed numerically also for several, different, operating conditions. Although the characteristic frequencies of the output signal change due to a different value of the speed of sound, the shape of the time response remains similar. Numerical results suggest that the time response of fast-response pressure probes operating with fluid flows that obey the perfect gas law are mainly affected by geometrical factors and by the value of β. When the probe is used to carry out measurements in flows of fluids in the non-ideal regime, very different dynamics characteristics of the line-cavity system are expected. Unlike ideal conditions, the output pressure signals are expected to show a significant dependency, in terms of damping variation and resonant frequency shift, on the thermodynamic state of the fluid.

3.2. Non-ideal flow

The response of the line-cavity system is evaluated for MDM vapor in two selected operating conditions, reported in Figure 3. The improved Peng-Robinson Stryjek-Vera (iPRSV) EoS [17] is used to model the thermodynamic behavior of the fluid. Although the iPRSV model does not represent the state-of-the-art among the possible thermodynamic formulations, it allows to capture, at least qualitatively, non-ideal phenomena that may arise within the flow field, at relatively low computational cost. Since the dynamics of the probe is mainly governed by wave propagation and reflection, non-ideal effects such as, for instance, a non-monotone variation of the speed of sound are expected to be key in defining the system response. According to the iPRSV model, operating conditions A and B lie in the ideal and non-ideal regime, with a value of Γ equal to 3.11 and 0.61 respectively.

Figure 3a depicts the non-dimensional step-response of the considered line-cavity system in operating conditions A (25 bar) and B (8 bar) for a small perturbation ($\beta \sim 1$). The predicted non-dimensional signals are very similar and

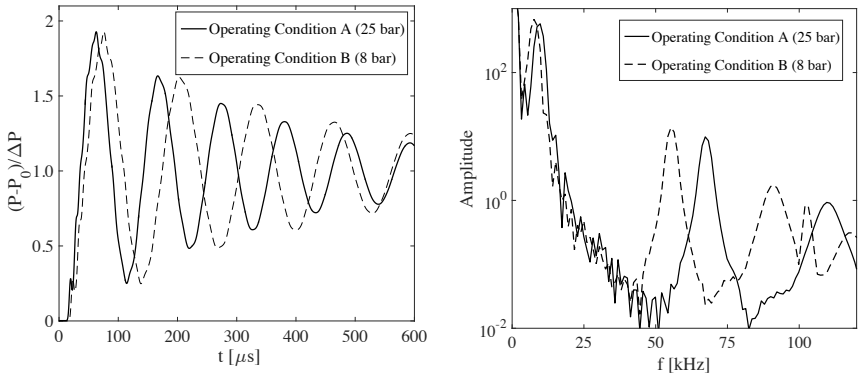

(a) Time step-response

(b) Step-response amplitude spectrum.

Op. Cond.	A	B
P [bar]	25	8
T [C]	310.3	270.5
c [m/s]	117.8	96.7
Γ	3.11	0.61
ν [mm^2/s]	0.186	0.136

Fig. 3: Non-dimensional step-response using MDM at 25 bar and 8 bar for an acoustic perturbation: β = 1.001 using the iPRSV EoS. The table reports the operating conditions for MDM (op. cond. A refers to TROVA experiment, whereas op. cond. B refers to the stator nozzle in [18]). The speed of sound values are computed using the iPRSV model.

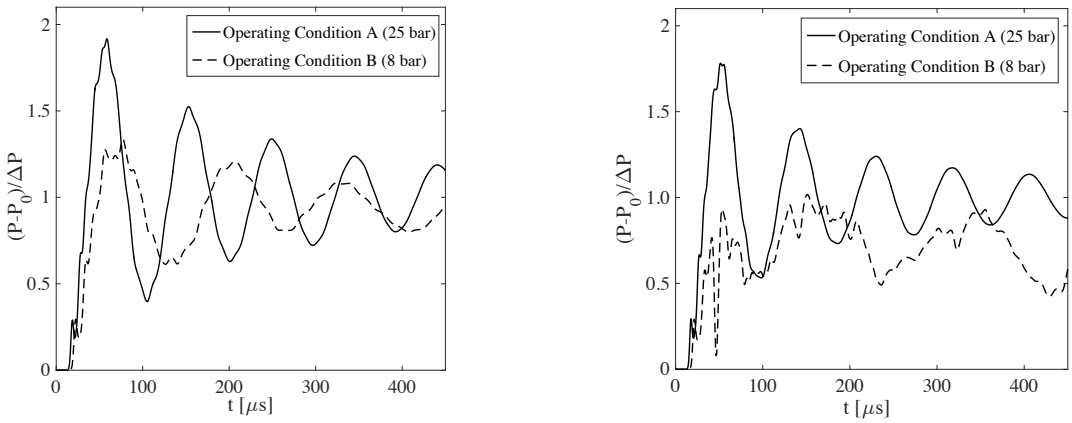

(a)

(b)

Fig. 4: System step response for an MDM vapor for different perturbation intensity. β = 1.1 (a); β = 1.2 (b)

poorly damped. Figure 3b reports the spectral analysis of the pressure signal for operating condition A and B. Results show that for operating conditions A the time response is characterized by higher harmonics: this was expected since the speed of sound is larger as reported in the table below figure 3. Second-order identification predicts a resonant frequency of 9.2 kHz and 7.6 kHz for operating conditions A and B, respectively. These values fairly agree with analytical predictions from equation (1), which returns 9.9 kHz and 8.5 kHz. Relative differences between numerical values and analytical predictions are comparable to that registered for dilute air, for a small perturbation (Figure 1b). Thus, numerical results suggest that thermodynamic non-idealities do not play a significant role in defining the line-cavity system response within the limit of acoustic perturbations. Indeed, the spectral density comparison of signal A against signal B, reported in Figure 3b, reveals that the energy is distributed similarly among the harmonics. Indeed, both signals present a steady contribution and a main peak corresponding to the resonant frequency. Secondary peaks are detected at 67 kHz (A) and 56 kHz (B) while tertiary peak are also found at higher frequency. As mentioned earlier, the bias between the corresponding amplitude peaks is due to the different value of the speed of sound. With f_{hf} the high-frequencies peaks, the ratio c/f_{hf} is constant for both operating conditions and for the acoustic response

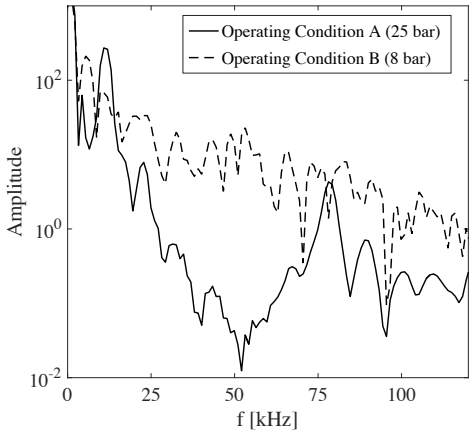

(a) Spectrum amplitude of the step-response with $\beta = 1.2$.

		$\beta = 1.1$	$\beta = 1.2$	$\beta = 1.3$
A	f_n [kHz]	10.0	10.8	11.6
	f_n (model) [kHz]	9.8	9.8	9.8
	ξ	0.08	0.10	0.13
	ξ_{nl} (correlation)	0.07	0.13	0.18
	ξ_v (Hougen)	< 0.01	< 0.01	< 0.01
B	f_n [kHz]	7.59	5.42	-
	f_n (model) [kHz]	8.5	8.5	-
	ξ	0.17	1.00	-
	ξ_{nl} (correlation)	0.16	0.29	-
	ξ_v (Hougen)	< 0.01	< 0.01	< 0.01

(b) Characteristics values from second-order identification are compare against analytical predictions from Eq. (1) (model) and (3) (correlation).

Fig. 5: Numerical results for a MDM vapor. Spectrum amplitude of the step-response for $\beta = 1.2$ (a) and a comparison of the characteristic values for different β(b).

of dilute air. This suggest that shape of the system response to a small acoustic perturbation does not depend on the properties of the fluid.

If larger pressure perturbations are considered, a different behavior is predicted. For instance, Figures 4a and 4b report the non-dimensional signals for $\beta = 1.1$ and $\beta = 1.2$, for a MDM vapor at operating conditions A and B. With particular reference to Figure 4a, besides the expected differences related to a different value of the speed of sound, numerical results reveal a significant variation of the damping factor. In particular, the response in non-ideal regime (operating condition B) is more damped than that of ideal regime, even though the same pressure ratio β is applied to the system. This difference is even more relevant for a value of $\beta = 1.2$, as showed in figure 4b. The response of the system in non-ideal regime is almost critically damped and it presents dramatic differences with respect of the signal resulting in the ideal regime. These differences are also observed from the comparison of the spectrum amplitude of pressure signals, reported in Figure 5a. Within the limit of acoustic waves, the amplitude spectrum was similar for different fluids both in ideal and non-ideal regimes. Different values of characteristics frequencies were possibly due to a different value of the speed of sound which is strictly related to the properties of the fluid and to its unperturbed conditions. If $\beta = 1.2$, the amplitude spectrum in non-ideal regime presents a very different trend: the energy is distributed almost uniformly, over a wide range of frequencies. There is not a clear separation between the main frequency peak and secondary high frequency peaks but the energy distribution instead keeps decreasing constantly as the harmonic frequency increases. The values of the resonant frequencies and of the non-dimensional damping ratios obtained from a second-order identification are reported in table 5b, for different values of β. In operating condition A, numerical results agree fairly well with analytical predictions for the resonant frequency and with the correlation (3) for the non-dimensional damping factor, although the latter is slightly overestimated. Second-order identification suggests that the damping is larger in operating condition B than operating condition A. This might be due to the very different value of the ratio $P/(\rho c^2)$, which is 0.56 for operating condition A and 1.47 for operating condition B. Indeed, this ratio enters the correlation (3) and is associated to the isentropic compressibility of the fluid. When considering operating condition B (non-ideal regime), the correlation (3) provides a good estimation for $\beta = 1.1$, while it fails significantly for $\beta = 1.2$. This is possibly due to non-ideal effects that result in negative variations of the speed of sound that goes from an unperturbed state value of 95.6 m/s to a perturbed state value of 85.6 m/s. This large negative speed of sound variation increases the isentropic compressibility of the fluid $1/(\rho c^2)$, i.e. entails larger values of damping. Furthermore, it causes a reduction of the main frequency. A thorough investigation of pressure probe dynamics, considering different geometries, working fluids and operating conditions is mandatory before enlarging the limits of the results presented in this work. Such an investigation is left for future works.

4. Conclusion

The step-response of a line-cavity system to non-acoustic pressure perturbations has been assessed and the analysis has been extended to the non-ideal regime of interest for ORC applications. The pertinent technology is fast-response pressure probes for pressure measurements past the turbine rotor. First, the role of non-linear terms has been assessed through several numerical simulations, involving dilute air, to investigate how the system response changes depending on the intensity of the perturbation. Indeed, the Hougen model predicts a constant damping factor while numerical results show that the damping factor instead increases as the pressure perturbation intensity increases. To this extent, a more generic expression for the non-dimensional damping factor is proposed. At the same time, numerical results suggest that non-idealities do not play a significant role within the limit of acoustic perturbations. When the acoustic perturbation assumption is relaxed, non-idealities are found to introduce even higher levels of damping. Analytical models and correlations calibrated with dilute air may be used with molecularly complex fluids in limit of the ideal regime. In the non-ideal regime, the estimation of line-cavity system dynamics is critical and depends on the values of the isentropic compressibility of the fluid and on the value of the fundamental derivative.

Acknowledgments

This research is supported by ERC Consolidator Grant N. 617603, Project NSHOCK, funded under the FP7-IDEAS-ERC scheme.

References

[1] Sharma, O.P., Pickett, G.F., Ni, R.H.. Assesment of unsteady flows in turbomachinery. ASME J Turbomachinery 1992;114:79–90.
[2] Miller, R.J., Moss, R.W., Ainsworth, R.W., Horwood, C.K.. Time-resolved vane-rotor interaction in a high-pressure turbine stage. ASME J Turbomachinery 2003;125:1–13.
[3] Schlienger, A., Kalfas, A.I., Abhari, R.S.. Vortex-wake-blade interaction in a shrouded axial turbine. ASME J Turbomachinery 2005;127.
[4] Gaetani, P., Persico, G., Dossena, V., Osnaghi, C.. Investigation of the flow field in a high-pressure turbine stage for two stator-rotor axial gaps-part ii: Unsteady flow field. ASME J Turbomachinery 2007;129:580–590.
[5] Porreca, L., Kalfas, A.I., Abhari, R.S.. Aero-thermal analysis of partially shrouded turbine blades. J Propulsion and Power 2009;25.
[6] Persico, G., Gaetani, P., Osnaghi, C.. A parametric study of the blade row interaction in a high pressure turbine stage. ASME J Turbomachinery 2009;131.
[7] Brouckaert, J.F.. Fast response aerodynamic probes for measurements in turbomachines. J of Power and Energy 2007;126.
[8] Persico, G., Gaetani, P., Guardone, A.. Design and analysis of new concept fast-response pressure probes. Meas Sci Technol 2005;16:1741–1750.
[9] Thompson, P.A.. A fundamental derivative in gasdynamics. Phys Fluids 1971;14(9):1843–1849.
[10] Gori, G., Molesini, P., Persico, G., Guardone, A.. Non-ideal compressible-fluid dynamics on fast-response pressure probes for unsteady flow measurements in turbomachinery. Journal of Physics Conference Series 2017;821.
[11] Palacios, F., Colonno, M.F., Aranake, A.C., Campos, A., Copeland, S.R., Economon, T.D., et al. Stanford University Unstructured (SU2): An open-source integrated computational environment for multi-physics simulation and design. In: 51st AIAA Aerospace Sciences Meeting and Exhibit. 2013,.
[12] Vitale, S., Gori, G., Pini, M., Guardone, A., Economon, T.D., Palacios, F., et al. Extension of the su2 open source cfd code to the simulation of turbulent flows of fuids modelled with complex thermophysical laws. In: 22nd AIAA Computational Fluid Dynamics Conference. AIAA Paper 2760; 2015,.
[13] Hougen, J.O., Martin, O.R., Walsh, R.A.. Dynamics of pneumatic transmission lines. Contr Eng 1963;.
[14] Doebelin, E.O.. Measurement systems: application and design. McGraw-Hill; 1990.
[15] Trusler, J.P.M.. Physical Acoustics and Metrology of Fluids. The Adam Hilger Series on Measurement Science and Technology; Bristol, England: Adam Hilger (IOP Publishing Ltd.); 1991.
[16] Lijung, L.. System Identification – Theory for the User. 2nd ed.; Upper Saddle River, NJ: Prentice Hall; 1999.
[17] Stryjek, R., Vera, J.H.. PRSV: An improved Peng-Robinson equation of state for pure compounds and mixtures. Can J Chem Eng 1986;64:323–333.
[18] Colonna, P., Rebay, S., Harinck, J., Guardone, A.. Real-gas effects in ORC turbine flow simulations: influence of thermodynamic models on flow fields and performance parameters. In: ECCOMAS CFD 2006. Egmond aan Zee, NL; 2006,.